Mincut Algorithm and Adaptive Histogram Equalization (AHE) for Segmentation of Retinal Layer in OCT Images with Choroidal Neovascularization

Miriam Zipporah* & N.Sharmila Banu**

*Research scholar, Department of Computer Science and Applications, Providence College for Women, Coonoor, Tamilnadu, INDIA.
E-Mail: miriamzipporah19{at}gmail{dot}com
**Assistant Professor, Department of Computer Science and Applications, Providence College for Women, Coonoor, Tamilnadu, INDIA.

***Abstract*—**Age-associated macular degeneration is one among the important reasons behind blindness. But, the intrinsic structures of retinas are complicated and hard to be identified owing to the neovascularization occurrence. Conventional surface detection techniques may face failure in the layer segmentation. In order to resolve this issue, the recent research presents supervised technique, which is suggested for simultaneous segmentation of the layers and neovascularization. However, the surfaces detection accuracy is restricted in layers where the contrast observed between layers is less and their boundaries are not notice able owing to the neovascularization occurrence. One more drawback of this research work is its need for high computing time. With the aim of solving these issues, contrast enhancement is carried out employing the Adaptive Histogram Equalization (AHE) and Min cut algorithm was also realized for the process. The longer processing time may be decreased through the parallelization of the newly introduced technique on segmentation of retina layers. The extraction of three spatial features, seven gray level based features and fourteen layer-like features are done for the Dense NET classifier. Thus the coarse surfaces of various OCT images can be found. For the description and enhancement of the retinal layers with diverse thickness and anomalies, multi-scale bright and dark layer detection filters are presented. A limited graph search algorithm is also introduced for the accurate detection of the retinal surfaces. It will be employed in the local region and it is more quick and provided results with more accuracy. The experimental outcomes indicate the newly introduced technique performs better than the benchmarked techniques.

***Keywords*—**Adaptive Histogram Equalization (AHE); Choroidal Neovascularization; Dense NET; Mincut Algorithm; OCT Images; Retinal.

***Abbreviations*—**Adaptive Histogram Equalization (AHE); Optical Coherence Tomography (OCT).

I. INTRODUCTION

OPTICAL coherence tomography (OCT) is a non-intrusive and non-contact imaging modality used for morphological evaluation and diagnosis of retinal abnormality, like AMD and glaucoma. The OCT images are frequently utilized for the diagnosis and monitoring of retinal diseases with more accuracy depending on abnormality quantification and computation of retinal layer thickness both in research centers and clinical routines (Wong et al 2014).

For the quantification of the thickness of retinal layers and volume of neovascularization, it is vital to design a robust and automated segmentation technique for both retinal layers and neovascularization as manual segmentation is a time consuming process for massive amount of OCT images used in clinical applications. But, numerous challenges are encountered. First, the inner structures of retinas are sophisticated and hard to be identified. Secondly, there might be irregularities like neovascularization and fluid. This results in low contrast and blurred edges in OCT images in between retinal layers, and also massive structural variations in the retinal layers. Layer segmentation may not succeed in making use of conventional surface detection techniques like conventional graph search algorithm (Shi et al 2014).

In order to get over the problems mentioned above, attention is paid on retinas segmentation with exudative AMD in OCT images that is related with neovascularization and probable fluid. Contrast enhancement is carried out by employing the Adaptive Histogram Equalization (AHE) and mincut algorithm was also realized for the process. The long processing time may be minimized by using the method proposed on segmenting the retina layers concurrently. The extraction of the three spatial features, seven gray level based features and fourteen layer-like features are done for the DenseNET classifier.

II. Literature Review

Abhishek et al [2014] suggested an automated segmentation algorithm for the detection of some intra-retinal layers that are necessary for Edema detection existing in SD-OCT images. An algorithm used for the precise segmentation of intra-retinal layers for normal persons and patients affected with edema is studied. The layers undergoing segmentation include Inner Limiting Layer (ILM) and Retinal Pigment Epithelium (RPE) layer. Then the thickness is measured and depending on the thickness the image is categorized to be edema or non-edema. The algorithm's accuracy is demonstrated to be greater than that of the standard edge based segmentation approaches that are more susceptible to the identification of fake and disjoint edges.

Xu et al [2014] introduced a work, which derives on an automated retinal blood vessel segmentation approach that is dependent on 3D SD-OCT and yields accurate vessel pattern for clinical analysis, retinal image registration, advance diagnosis and monitoring of the advancement of glaucoma and other retinal diseases. The method of the invention makes use of a machine learning algorithm for the automatic identification blood vessel on 3D OCT image, in a way, which does not depend on and can neglect any other processing. The method can consist of two elements, (i) training of the algorithm and (ii) execution of the trained algorithm

Kanagasingam et al [2014] explained about various imaging modalities, which are presently being considered or utilized for the screening of Age-related Macular Degeneration (AMD). In addition, the available telemedicine studies that include diagnosis and treatment of AMD are also reviewed, and the way in which automated disease grading could be advantageous to telemedicine is studied. Since no treatment is available for dry AMD and just advance treatment can avoid the late AMD, mass screening via a telemedicine platform for facilitating early detection of AMD is emphasized.

Duan et al [2015] introduced a new technique for the segmentation of retinal layers in OCT images. The technique proposed makes use of a coarse-to-fine scheme for segmentation and consists of: (1) A variational retinex model, which can improve the details in addition to correcting the in-homogeneities in intensity; (2) An anisotropic coherent improving diffusion, which can eliminate speckle noise and connect the disrupted retinal layers simultaneously; (3) A nonlinear isotropic filter, which smoothens the processed OCT image and results in the initial coarse segmentation; (4) A high-pass unsharp masking filter, which focuses on the rest of the layers and provides a refined segmentation. Then, all of the retinal layers, which can be observed by human eyes are segmented with accuracy employing common edge detection of region based segmentation algorithms. Elaborate experimental results help in validating the efficiency and performance of the newly introduced technique.

Fang et al [2017] demonstrated a new framework that combines Convolutional Neural Networks (CNN) and Graph Search methods (CNN-GS) for the automated segmentation of nine layer boundaries on retinal OCT images. CNN-GS first makes use of a CNN for extracting the features of particular retinal layer boundaries and training an associated classifier for delineating a pilot estimate of the eight layers. Then, a graph search technique makes use of the probability maps generated from the CNN to get the boundaries finally.

Dodo et al [2017] suggested a simple but effective and computationally inexpensive technique of employing fuzzy histogram hyperbolization for enhancement method, and continuous max-flow for segmentation of four retinal layers (Inner Limiting membrane, Retinal Nerve Fibre Layer, Outer segment and the Retinal Pigment Epithelium). The results indicate increase in the performance of segmentation.

Luo et al [2017] attempted to look for the most appropriate edge detectors that can be used for the retinal OCT image segmentation task. The three most potential edge detection algorithms were found in the associated literature, which include canny edge detector, the two-pass technique, and the Edge Flow method. Moreover, the mean localization deviation metrics reveal that the two-pass technique produced the problem of smallest edge shifting. A better performance on an overall derived from Canny and two-pass techniques compared to Edge Flow method shows that the OCT images have more intensity gradient information rather than texture variations along the retinal layer boundaries.

Xiang et al [2018] provided a review on few significant image segmentation techniques used for the processing of the retinal OCT images may classify the OCT segmentation approaches into five distinct groups according to the image domain subjected to the segmentation algorithm. The present research works in OCT segmentation are generally dependent on enhancing the accuracy and precision, and on minimizing the necessary processing time. There is no question that the present 3-D imaging modalities are now shifting the research attempts towards volume segmentation in addition to 3-D rendering and visualization. It is also vital to design reliable techniques that have the capability of tackling with pathologic cases in OCT imaging.

III. Proposed Methodology

Contrast enhancement is performed by using the Adaptive Histogram Equalization (AHE) and mincut algorithm was also implemented for the process. The long processing time may be reduced by parallelizing proposed method on segmentation of retina layers. Three spatial features, seven gray level based features and fourteen layer-like features are extracted for the DenseNET classifier. The coarse surfaces of different OCT images can be thus found. To describe and enhance retinal layers with different thickness and abnormalities, multi-scale bright and dark layer detection filters are introduced. It will be used in the local region and faster and more accurate results will be obtained. In this research work, a new supervised segmentation framework is introduced for dealing with the before mentioned issues faced in the segmentation module of the retinal neovascularisation treatment. As illustrated in Figure 1, the newly introduced framework consists of two phases, which include: training phase and testing phase. In the training phase, manual annotation of OCT images are performed and then the features extraction are carried out for the training of the DenseNET classifier. During the testing phase, the proposed segmentation framework specifies a coarse-to-fine segmentation procedure, which comprises of three steps, which include preprocessing, image enhancement, initialization and segmentation employing clustering. The final surfaces are then refined with the help of a layer constrained graph searching algorithm and neovascularisation segmentation is also done. The architecture of the above proposed system has been illustrated in the figure 1.

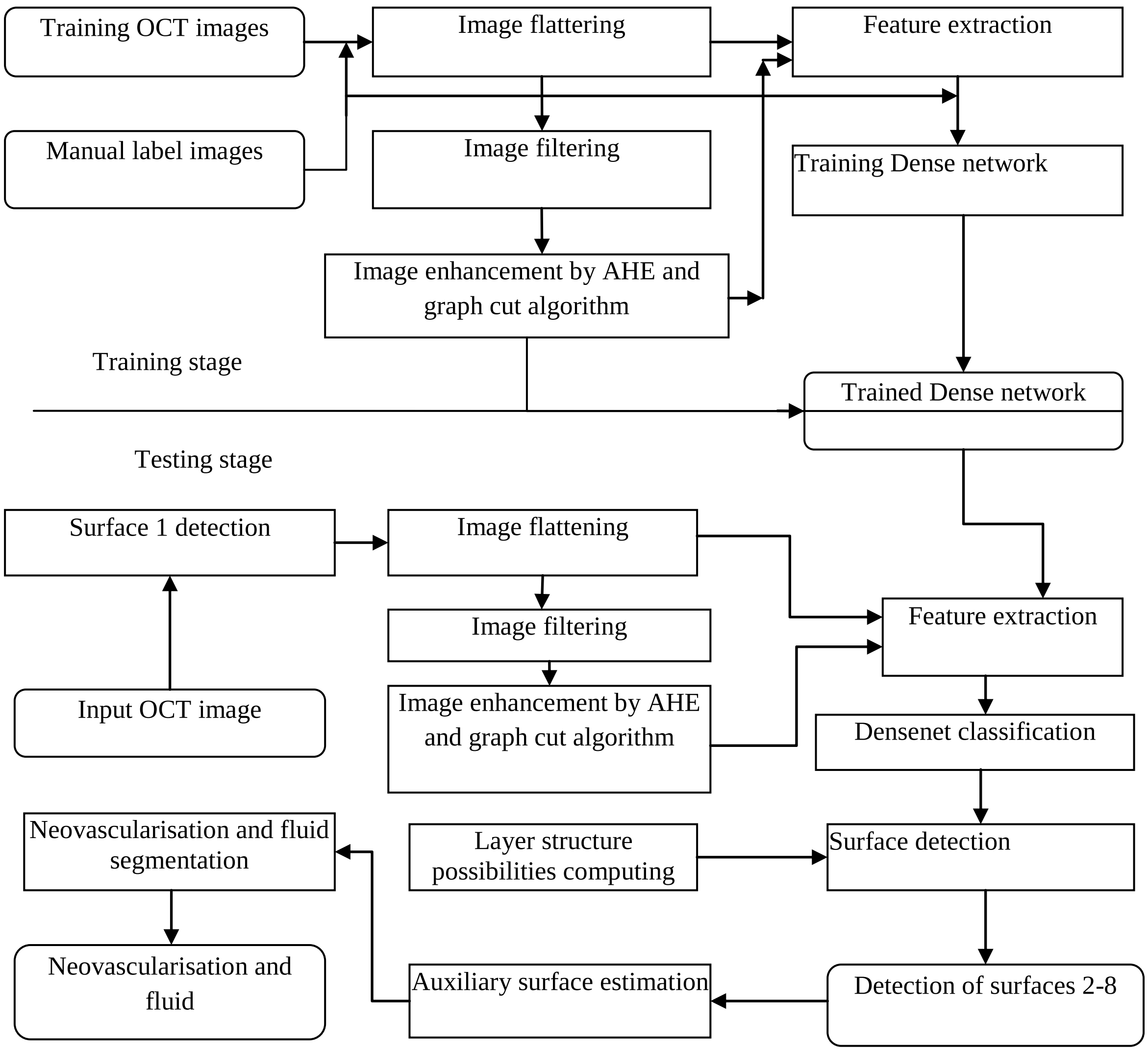

Figure 1: Proposed System Architecture

3.1. Image Filtering

In order to minimize the impacts of the eye movement, image flattening is frequently used for correcting the abnormal displacements (Garvin et al 2009). Surface 1 refers to the top interface existing between the vitreous and retina. For flattening a training or testing OCT image, Surface 1 has to be identified. During the training phase, the manually annotated image is scanned along the A-line for finding the interface between vitreous and NFL as Surface 1. In testing phase, initial Surface 1 is fast identified. First, noise smoothing is carried out slice after slice through the convolution of the B-scan images of the actual 3D OCT image with a Gaussian kernel of dimensions $\ell x \ell = 9x9$, mean $\mu = 0$ and standard variance $\sigma = 1{:}0$. Secondly, the voxel intensities of the smoothened image are changed in accordance with the below gray-level global transformation function:

$$(\vec{x}) \quad (\vec{x}) \quad (\vec{x}) \quad \text{—} (I_f(\vec{x}) \quad); \quad (\vec{x}) \quad 0; \quad I_f(\vec{x}) \leq I \tag{1}$$

Where, $\vec{x}$represents the voxel coordinates, IN ($\vec{x}$) refers to the normalized intensity of a voxel, If ($\vec{x}$) stands for the intensity of a voxel in the smoothened image,$I_{f,r}$refers to the normalized range, the intensity interval is [I],I stands for the maximal normalized intensity. In the experiments, is computed by the minimal value $I_{f,min}\overrightarrow{(x)}$ and the maximal value $\overrightarrow{(x)}$ of the smoothed image, i.e, $\overrightarrow{(x)}$ $(I_{f,max}\overrightarrow{(x)}$ $\overrightarrow{(x)}), \tau_f$is fixed to 0.25, and I is fixed to the maximal value$I$ $\overrightarrow{(x)}$. is fixed to 255. Canny edge detection algorithm is utilized for obtaining the initial Surface 1. The multi-resolution graph search algorithm [45] is utilized for detecting the Surface 1 based on initial Surface 1. In training and testing phase, voxels below the Surface 1 in every line are top aligned for flattening images.

3.2. Adaptive Histogram Equalization (AHE)

Adaptive histogram equalization (AHE) makes use of the HE mapping function that is supported over a particular size of a local window to decide every density value that is enhanced. It functions as a local operation. Hence, the regions that occupy various gray scale ranges can be improved at the same time. As stated in the first section, its performance is very belligerent that in considerably homogeneous areas, the noise gains prominence. In the form of the sole parameter, the size of the local window has a control over the trade-off existing between local enhancement and noise amplification. The AHE algorithm is computationally intensive and interpolation version is generally brought into use. On the other side, multi-scale analysis disintegrates a signal into multiple spatial-frequency components. Through the proper selection of the decomposition filters, the necessary features of an object can be isolated from noise. Hence, the features of interest can be selectively enhanced by transforming the respective components in the transform domain.

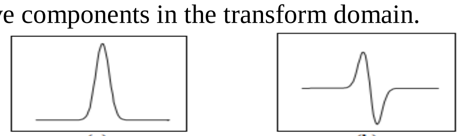

Figure 2: (a) Cubic spline smoothing function θ(x). (b) Quadratic spline wavelet ψ(x) of compact support defined to be the derivative of the smoothing function

For this research work, the quadratic spline wavelet function ψ(x) is used that has little support and is consistently differentiable. It is regarded to be the derivative of a cubic spline function θ (x) (Figure 2). It can be demonstrated that by making use of a wavelet, which is the derivative of a smoothing function the wavelet transform of the signal f is in proportion to the derivative of the signal that is smoothed at scale 2j. Then the wavelet transform can be regarded to be an adaptive (scale based) detection process, which gets the signal variation points in two orthogonal directions x and y. Moreover, the wavelet function used, as illustrated in Figure 2 (b), well approximates the first derivatives of a Gaussian function. In this research work, the contrast enhancement is introduced by AHE in a multi-scale paradigm. Based on the frequency characteristics of the sub-band images generated due to expansion, AHE is apply with various sizes of local windows. A number of factors are considered while selecting the appropriate size of local windows for AHE processing within the sub-band images.

(1) The frequency characteristics of the sub-band. The coarser levels have more typical shape information and must not be modified much. Hence, a considerably large size local window is applied. On the other side, the finer levels have much of local detail information. So, considerably compact local windows are brought into use. In the application, the dyadic wavelet decomposition was employed; hence the local window size is chosen so to match with the dyadic series that was used for supporting the decomposition filters.

(2) The size of the image. Discrete histogram equalization is just an approximation of the analytical case, hence when the number of pixels used for computation of the histogram is smaller, and then the result will not have stability and will possess a massive deviation from what is theoretically expected. In addition, the size of the image also decides the maximum levels in dyadic wavelet decomposition.

3.3. Mincut Algorithm

Graph connectivity is one among the conventional subjects in graph theory, and has several practical applications, for instance, in chip and circuit design, robustness of communication networks, transportation planning, and cluster analysis. Getting the minimum cut of an undirected edge-weighted graph is a basic algorithmically problem. Actually, it involves getting a nontrivial partition of the graphs vertex set V into two parts so that the cut weight, the sum of the weights of the edges that connect the two parts, is minimal.

The Algorithm

All through the research work, a simple undirected graph G with vertex set V and edge set E is involved. Each edge e has nonnegative real weight w (e). One simple key observation is the way in which two vertices s and t, and the weight of a minimum s-t-cut are found:

THEOREM 1. Let s and t refer to the two vertices of a graph G. Let G/{s, t} stand for the

Graph achieved by combining s and t. Then a minimum cut of G can be got by considering the smaller of a minimum s-t-cut of G and a minimum cut of G/{s, t}.

The theorem is true as either there exists a minimum cut of G, which differentiates s and t, then a minimum s-t-cut of G is a minimum cut of G; or there is none, then a minimum cut of G/{s, t} performs the task. Therefore, a procedure that finds a random minimum s-t-cut can be utilized or constructing a recursive algorithm to get a minimum cut of a graph. The algorithm below, called in the literature as maximum adjacency search or maximum cardinality search, gives the necessary s-t-cut.

MINIMUMCUTPHASE (G, w, a)

{ }

While$A$

To A is added the most strongly connected vertex and the cut-of-the-phase is stored and G is shrunk by integrating the two vertices that are added last A subset A of the graphs vertices grows starting with an arbitrary single vertex until A is equal to V. In every step, the vertex external to A that is most strongly connected with A is added. Formally, a vertex is added

$$w(A,z) \quad \{ \ (\quad y)| \quad A\}, \quad (2)$$

Where w (A, y) refers to the sum of the weights of all of the edges between A and y. At the finale of every such stage, the two vertices that are added finally are combined, that is, the two vertices are substituted by a new vertex, and any edges from the two vertices to a remaining vertex are substituted by an edge weighted by the summation of the weights of the earlier two edges. Edges that join the merged nodes are eliminated. The cut of V, which isolates the vertex added finally from the remaining portion of the graph, is known as the cut-of-the-phase. The lightest of these cuts-of-the-phases becomes the result of the algorithm, the necessary minimum cut:

MINIMUMCUT (G, w, a)

While$|V|$

MINIMUMCUTPHASE (G, w, a)

If the cut-of-the-phase is lighter compared to the current minimum cut

Then store the cut-of-the-phase to be the current minimum cut

It is to be noticed that the beginning vertex a remains the same throughout the entire algorithm. It can be chosen in random in every phase.

3.4. Feature Extraction

The objective of the feature extraction phase is pixel characterization using a feature vector, which is a pixel representation in terms of few quantifiable metrics that may be easily utilized in the classification phase to determine if the pixels belong to an actual blood vessel or not. In this research work, the below sets of features were chosen.

- *Gray-level-based features*: features that depend on the dissimilarities between the gray-level in the candidate pixel and a statistical value that represents its environment.
- *Moment invariants-based features*: features depending on moment invariants for defining the small image regions created by the gray-scale values of a window that are entered on the pixels represented.

1) Gray-Level-Based Features: As the blood vessels are always darker compared to their surroundings, the features that depend on the description of the gray-level change in the surroundings of candidate pixels is a desired preference. A group of gray-level-based descriptors considering this information were obtained from homogenized images that take just a small pixel region the cantered on the defined pixel stands for the set of coordinates in a sized square window centred on point Then, these descriptors can be defined as

$$(x,y) = I_H(x,y) \quad \underset{(s,t)\in}{} \quad \{ \quad (s,t)\} \quad (3)$$

$$(x \ y) \quad \underset{(s,t)\in}{} \quad \{ \quad (s,t)\} \quad (x \ y) \quad (4)$$

$$(x \ y) \quad (x \ y) \quad \underset{(s,t)\in}{} \quad \{ \quad (s,t)\} \quad (5)$$

$$(x \ y) \quad \underset{(s,t)\in}{} \quad \{ \quad (s,t)\} \quad (6)$$

$$(x \ y) \quad (x \ y) \quad (7)$$

2) Moment Invariants-Based Features: The vasculature in retinal images is observed to be piecewise linear and its approximation can be done by several line segments that are connected. For the detection of these quasi-linear shapes that are not all wide equally and whose orientation may be at any angle, shape descriptors invariant to

Translation, rotation and scale variations may have a significant role to play. In this technical work, they are computed as below. The size of this region was set to 17*17 such that, with that the region is centred on the middle of a "wide" vessel (8-9-pixel wide and called to retinas of approximately 540 pixels in diameter), the subimage has an approximately equivalent number of vessel and no vessel pixels. For this sub image, represented as b, the 2-D moment of order is expressed as,

$$\sum\sum i \quad (i,j) \quad (8)$$

Where the summations are computed over the values of the spatial coordinates i and j spanning the subimage, and is$I_{VE}^{x,y}(i,j)$ the gray-level at point (i,j). A set of seven moment invariants under size, translation, and rotation, referred as Hu moment invariants, can be obtained from the combinations of regular moments. Amongst them, the tests have shown only those expressed by,

$$(x \ y) \quad \mathrm{og}(\phi_1) \quad (9)$$

$$(x,y) = \log(\phi_2) = (\eta_{20} + \eta_{02}) \quad (10)$$

Including the remainder moments lead to reducing classification performance and maximized computation required for classification. In addition, the module of the logarithm was utilized rather than its values themselves. Making use of the logarithm minimizes the dynamic range and the module avoids from having to tackle with the complex numbers due to the computation of the logarithm of negative moment invariants.

3.5. Dense Net

Take a single imagex_0, which is passed through a convolutional network. The network consists of L layers, each one of which realizes a non-linear transformation Hι(·), where ℓ is the index of the layer. Hι(·) could be a composite function of operations like Batch Normalization (BN) (Ioffe and Szegedy,2015), rectified linear units (ReLU) (Glorot et al

2011), Pooling (LeCun et al 1998), or Convolution (Conv) the output of the ℓ th layer as x_ℓ.

ResNets. Conventional convolutional feed-forward networks connect the output of the ℓth layer to be the input to the (ℓ + 1) th layer (Krizhevsky et al 2012) that yields the below layer transition: $x_\ell = H_\ell(x_\ell - 1)$. ResNets (He et al 2016) adds a skip-connection, which bypasses the non-linear transformations using an identity function:

$$= H_\ell\,(x_\ell - 1) + x_\ell - 1 \quad \ldots \qquad (11)$$

One benefit of ResNets is that the flow of the gradient is direct through the identity function from the layers aftermath to the previous layers. But, the identity function and the output of H_ℓ are merged by summation that may interrupt the flow of information in the network.

Dense connectivity. In order to further enhance the information flow between layers another connectivity pattern is proposed: a direct connection is introduced from any layer to every subsequent layer. Figure 3 shows the schematic layout of the resultant Dense Net.

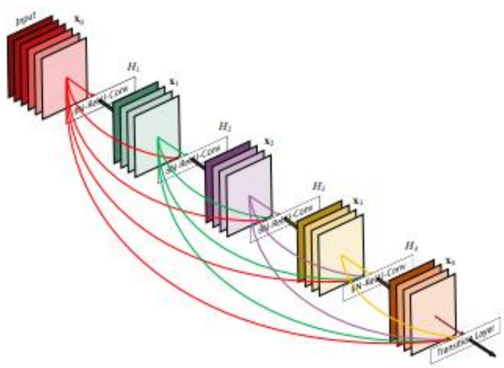

Figure 3: A 5-layer dense block with a growth rate of k = 4. Every layer considers all preceding feature-maps to be the input

As a result, the ℓth layer obtains the feature-maps of every preceding layer, $x_0 \ldots x_\ell - 1$, in the form of input:

$$x_\ell = H_\ell([x_0, x_1, \ldots, x_\ell - 1]) \qquad (12)$$

Where $[x_0 \ldots x_\ell - 1]$ indicates the concatenation of the feature-maps generated in layers 0, . . ., ℓ−1. Due to its dense connectivity, this network architecture is referred as Dense Convolutional Network (DenseNet). For easy implementation, the multiple inputs of $H_\ell(\cdot)$ in eq. (4.12) is concatenated into one single tensor.

Composite function. Inspired by (He et al 2016), Hℓ(·) is define as a composite function of three consecutive operations: batch normalization (BN), which is then followed by a rectified linear unit (ReLU) and a 3 × 3 convolution (Conv).

Pooling layers. The concatenation operation employed in Eq. (12) is not feasible if there is a change in the size of feature-maps. But, one important part of convolutional networks is the down-sampling layers, which modify the size of feature-maps. To enable down-sampling in this architecture, the network is divided into several densely connected dense blocks; Figure 4 illustrates.

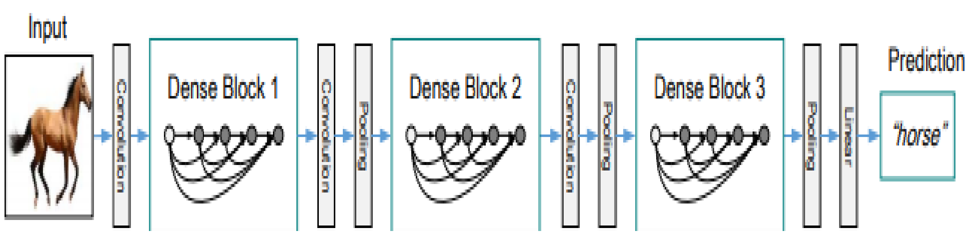

Figure 4: A deep DenseNet with three dense blocks. The layers between two adjacent blocks are called as transition layers and changes feature-map sizes through convolution and pooling

The layer between blocks is also referred as transition layers that perform convolution and pooling. The transition layers utilized in experiments comprises of a batch normalization layer and a 1×1 convolutional layer, which is then followed by a 2×2 average pooling layer. Growth rate. If every function Hℓ generates k feature maps, it follows that the ℓ th layer has k0 +k × (ℓ−1) input feature-maps, where k0refers to the number of channels in the input layer. One significant difference between DenseNet and the available network architectures is that DenseNet can possess very narrow layers, e.g., k = 12. The hyperparameter k is referred to as the growth rate of the network. It can explained is that every layer can access all the preceding feature-maps present in its block and, hence, the network's "collective knowledge" also. One can see the feature-maps to be the network's global state. Every layer adds its own k feature-maps to this state. The growth rate controls how much amount of new information is contributed by every layer to the global state. Once written, the global state can be accessed from any place within the network and, dissimilar to conventional network architectures; it is not needed to have it replicated from one layer to another.

3.6. *Constrained Graph Search for Surface Detection*

The graph search algorithm is utilized for refining the positions of the vertices in the initial surfaces. In comparison with the earlier work (Tian et al 2015), a novel cost function is devised depending on layer structure detection, helping in the identification of the optimal surfaces of retinal layers although the contrast between the adjacent layers is low and morphological variations of retinal layers are huge owing to neovascularisation and fluid. Like it is designed in the LOGISMOS framework (Li et al 2006), optimal surface detection can be modified into getting a minimum-cost closed set in the respective vertex-weighted graph. Shortly, this comprises of two essential tasks. First, Surfaces 2-6 were identified by the constraints of Surface 7. Secondly, the correct formulation of a cost function needs to be provided as it provides a measure of the possibility that every node in the graph belongs to a specific surface, and decides on the optimal surface with the least cost. Hence, a correct initialization of surfaces and an enhanced cost function helps in detecting the surfaces with more accuracy in OCT images with diseases compared to the earlier techniques.

3.7. Neovascularisation Segmentation

The layers under Surface 7 are at times are locally distorted upwards around neovascularisation. Fluid due to neovascularisation occurs frequently. In order to identify the neovascularisation and fluid, the positions has to be estimated. This is performed through the computation of the height of the deformed surfaces and the fluid occurrence. Surface 7 varies suddenly and is deformed in the abnormal region whereas its actual pre-disease position is a smooth surface. For every curve of Surface 7 in every B-scan, the respective bottom contour is computed through the convex hull algorithm. The footprints of the deformed Surface 7 can be observed through the scanning of every curve of Surface 7 and its bottom contour in every B-scan. The pixel is taken in the footprints of the abnormal region when the distance between Surface 7 and its bottom contour is greater compared to a threshold value (twenty-voxels height). Then neovascularisation and fluid are segmented restrained by the footprint of the irregular region.

IV. Results and Discussion

In this system deals with comparison analysis of existing neural network classifier and proposed Adaptive Histogram Equalization (AHE) and mincut algorithm was also implemented for the process. The figure 5 shows the input OCT image with neovascularisation. The **s**urface detection accuracy is limited in layers where the contrast between layers is low and their boundaries are not visible due to the occurrence of neovascularization with the help of existing neural network segmentation. The figure 6 shows the Multiscale bright dark detection results were computed for input image. Figure 7 shows the testing image of the proposed system computed from the bright dark detection results Figure 8 shows the noise removal results of the proposed Adaptive Histogram Equalization (AHE) with densNet classifier.

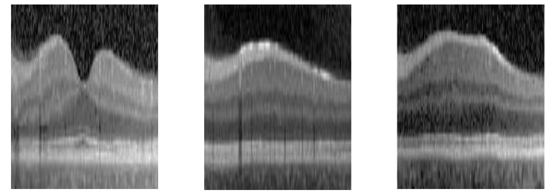

Figure 5: The Input OCT Image with Neovascularisation

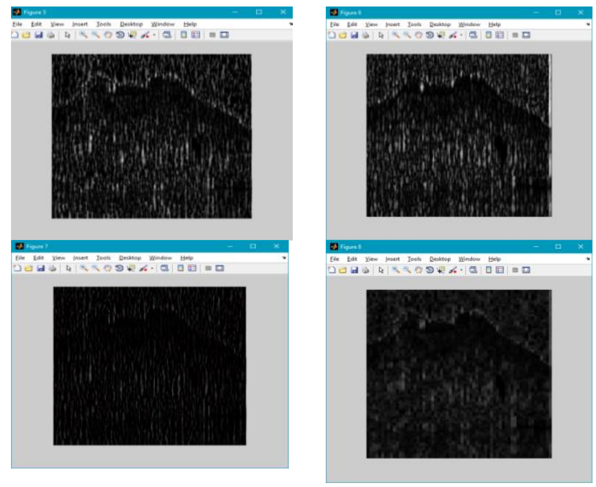

Figure 6: Multiscale Bright Dark Detection Results

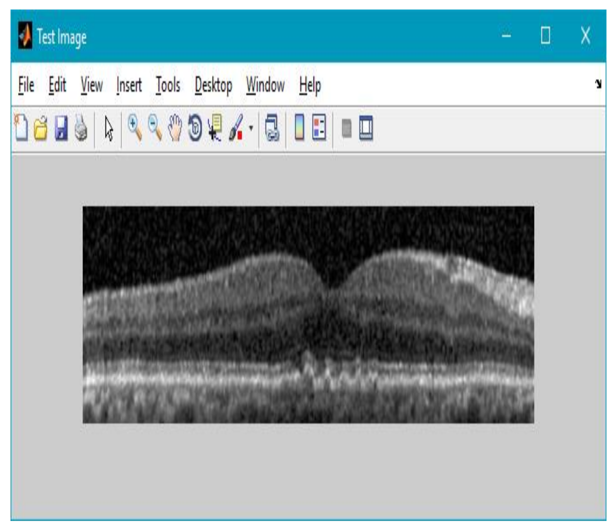

Figure 7: Test Image

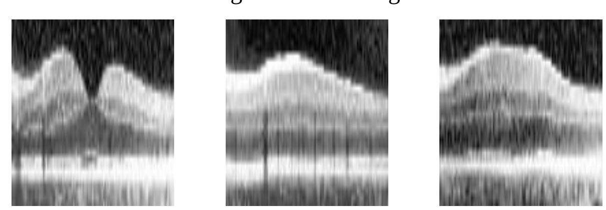

Figure 8: Results of the Proposed AHE for Test Image

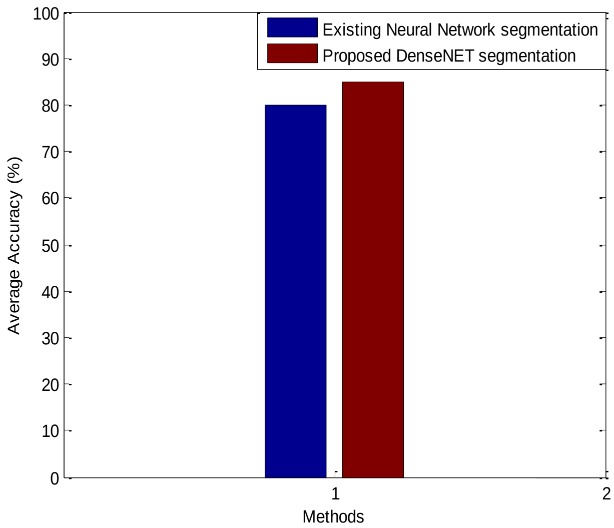

Figure 9: Performance Segmentation between Existing and Proposed System

The figure: 9. shows the comparison results of the performance segmentation between neural network and DensNet segmentation. It concludes that the proposed DensNet segmentation used in the local region and faster and more accurate results will be obtained and the average accuracy is 85%which is 5%, higher when compared to existing neural network segmentation respectively.

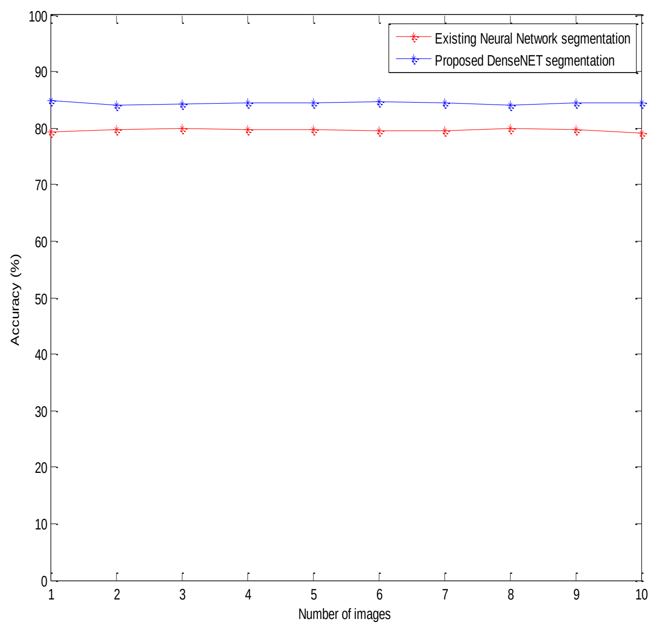

Figure 10: Performance Accuracy between Existing and Proposed System

Figure 10 the comparison results of the performance accuracy between neural network and DensNet segmentation. It concludes that the proposed DensNet segmentation produces more accurate results will be obtained and the accuracy is 85.67%where the existing neural network accuracy is 79.06%. So the experimental results shows that the proposed method outperforms state-of-the-art methods

V. Conclusion and Future Work

In this work, one new method introduces a supervised method is reported for simultaneously segmenting layers and neovascularization. The Adaptive Histogram Equalization (AHE) the bright layer possibility and the dark layer possibility were computed serially from small scale to large scale and mincut algorithm was also implemented for the process. The long processing time may be reduced by parallelizing proposed method on segmentation of retina layers. Three spatial features, seven gray level based features and fourteen layer-like features are extracted for the DenseNET classifier is implemented with feature integration module at different level of hierarchy in the deep nets and the main reason is to enhance feature learning due to loss of details. In future work, Regularization of the network is quite an important field for a successful image analysis framework with deep nets. Therefore, dropout mechanisms with adaptive optimization algorithms (such as ADAM instead of pure SGD) should be used.

References

[1] Abhishek, A.M., Berendschot, T.T., Rao, S.V. and Dabir, S., 2014, Segmentation and analysis of retinal layers (ILM & RPE) in Optical Coherence Tomography images with Edema. IEEE Conference on Biomedical Engineering and Sciences (IECBES), pp. 204–209.

[2] Dodo, B.I., Li, Y. and Liu, X., 2017, Retinal OCT image segmentation using fuzzy histogram hyperbolization and continuous max-flow. IEEE International Symposium on Computer-Based Medical Systems (CBMS), pp. 745–750.

[3] Duan, J., Tench, C., Gottlob, I., Proudlock, F. and Bai, L., 2015, Optical coherence tomography image segmentation. IEEE International Conference on Image Processing (ICIP), pp. 4278–4282.

[4] Fang L., Li S., Cunefare D., Farsiu S., "Segmentation based sparse reconstruction of optical coherence tomography images," IEEE Trans. Med. Imaging 36(2), 407–421 (2017).

[5] Garvin M. K., M. D. Abramoff, X. Wu, S. R. Russell, T. L. Burns,and M. Sonka, "Automated 3-d intraretinal layer segmentation of macular spectral-domain optical coherence tomography images," IEEE transactions on medical imaging, vol. 28, no. 9, pp. 1436–1447, 2009.

[6] Glorot X., A. Bordes, and Y. Bengio. Deep sparse rectifier neural networks. In AISTATS, 2011.

[7] He K., X. Zhang, S. Ren, and J. Sun. Deep residual learning for image recognition. In CVPR, 2016.

[8] He K., X. Zhang, S. Ren, and J. Sun. Identity mappings in deep residual networks. In ECCV, 2016.

[9] Ioffe S. and C. Szegedy. Batch normalization: Accelerating deep network training by reducing internal covariate shift. In ICML, 2015.

[10] Kanagasingam, Y., Bhuiyan, A., Abràmoff, M.D., Smith, R.T., Goldschmidt, L. and Wong, T.Y., 2014. Progress on retinal image analysis for age related macular degeneration. Progress in retinal and eye research, 38, pp.20–42.

[11] Krizhevsky A., I. Sutskever, and G. E. Hinton. Imagenet classification with deep convolutional neural networks. In NIPS, 2012.

[12] LeCun Y., L. Bottou, Y. Bengio, and P. Haffner. Gradientbased learning applied to document recognition. Proceedings of the IEEE, 86(11):2278–2324, 1998.

[13] Li K., X. Wu, D. Z. Chen, and M. Sonka, "Optimal surface segmentation in volumetric images-a graph-theoretic approach," IEEE transactions on pattern analysis and machine intelligence, vol. 28, no. 1, pp. 119–134, 2006.

[14] Luo, S., Yang, J., Gao, Q., Zhou, S. and Zhan, C.A.A., 2017. The edge detectors suitable for retinal OCT image segmentation. Journal of healthcare engineering, Volume. 2017, no. 3978410, pp.1–13.

[15] Shi F., X. Chen, H. Zhao, W. Zhu, D. Xiang, E. Gao, M. Sonka, and H. Chen, "Automated 3-d retinal layer segmentation of macular optical coherence tomography images with serous pigment epithelial detachments," IEEE transactions on medical imaging, vol. 34, no. 2, pp. 441–452, 2015.

[16] Tian J., B. Varga, G. M. Somfai, W.-H. Lee, W. E. Smiddy, and D. C. DeBuc, "Real-time automatic segmentation of optical coherence tomography volume data of the macular region," PloS one, vol. 10, no. 8, p. e0133908, 2015.

[17] Wong W. L., X. Su, X. Li, C. M. G. Cheung, R. Klein, C.-Y. Cheng, and T. Y. Wong, "Global prevalence of age-related macular degeneration and disease burden projection for 2020 and 2040: a systematic review and meta-analysis," The Lancet Global Health, vol. 2, no. 2, pp. e106–e116, 2014.

[18] Xiang, D., Tian, H., Yang, X., Shi, F., Zhu, W., Chen, H. and Chen, X., 2018. Automatic Segmentation of Retinal Layer in OCT Images With Choroidal Neovascularization. IEEE Transactions on Image Processing, Vol.27, no. 12, pp. 5880 – 5891.

[19] Xu, J., Tolliver, D., Ishikawa, H., Wollstein, C.G. and Schuman, J.S., Carnegie-Mellon University and University of Pittsburgh, 2014. Blood vessel segmentation with three-dimensional spectral domain optical coherence tomography. U.S. Patent 8,831,304.